Applied Catalysis B: Environment and Energy 344 (2024) 123607

Contents lists available at ScienceDirect

Applied Catalysis B: Environment and Energy

journal homepage: www.elsevier.com/locate/apcatb

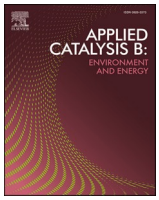

Exploration of the Mn-O coordination regulated reaction stability of manganese oxides in NH_3-SCR: Effect of deposited ammonium nitrates

Wang Song [a], Qianni Cheng [b], Li Han [a], Jiawei Ji [a], Yandi Cai [b], Wei Tan [b], Jingfang Sun [c], Changjin Tang [d,e,*], Lin Dong [a,b,c,**]

[a] School of Chemistry and Chemical Engineering, Laboratory of Mesoscopic Chemistry of MOE, Nanjing University, Nanjing 210093, China
[b] School of Environment, Nanjing University, Nanjing 210093, China
[c] Key Laboratory of Vehicles Emission Control of Jiangsu Province, Center of Modern Analysis, Nanjing University, Nanjing 210093, China
[d] School of Environment, Nanjing Normal University, Nanjing 210023, China
[e] Jiangsu Province Engineering Research Center of Environmental Risk Prevention and Emergency Response Technology, Nanjing 210023, China

ARTICLE INFO

Keywords:
Low-temperature NH_3-SCR
Reaction stability
MnO_x catalysts
Deposited ammonium nitrates
Coordination configuration

ABSTRACT

Manganese oxide-based catalysts exhibit excellent low-temperature denitration efficiency, making them potential candidates for application. Herein, the relationship between reaction stability and phase structure for MnO_2, Mn_2O_3 and Mn_3O_4 was disclosed. The NO conversion for Mn_2O_3 drastically reduced after 120 h reaction, while minor decline was detected for MnO_2 and Mn_3O_4. Based on dedicate qualitative and quantitative analyses on the deposits over catalyst surface, deactivation trigged by ammonium nitrate (AN) deposition was confirmed. Different from penta-coordinated Mn^{4+} on MnO_2 (110) and tri-coordinated Mn^{2+}, penta-coordinated Mn^{4+} on Mn_3O_4 (101), the unique tetra-coordinated Mn^{3+} on Mn_2O_3 (200) could stabilize the nitrates and make it difficult to be removed via decomposition or reaction and accumulate continuously, which resulted in the significant deactivation. This research could not only unveil the poisoning mechanism of MnO_x based catalysts, but also provide new insights into the relationship between the catalytic stability and surface Mn-O microstructure.

1. Introduction

NO_x (i.e. NO and NO_2) are major air contaminants that pose great risk to human health and ecology system. Selective catalytic reduction of NO_x with NH_3 (NH_3-SCR) is currently the most widely applied approach for NO_x elimination [1,2]. To avoid catalyst deactivation stimulated by high dust and sulfur, the installation of SCR denitration system after electrostatic precipitator and desulfurization units is suggested. Unfortunately, traditional V_2O_5-WO_3(MoO_3)/TiO_2 catalysts are inadequate to accomplish this task due to the inferior NO conversion efficiency at low temperature (< 150 ℃) [3]. Given the enormous energy consumption for reheating flue gas, it is urgent to develop NH_3-SCR catalysts with excellent performance at low temperatures.

Among diverse metal transition oxides, manganese oxides (MnO_x) display excellent catalytic efficiency for NO_x removal [4–7]. In general, the activity of MnO_x is outstanding, which can fulfill full NO conversion even at the low temperature of 100 ℃ [8,9]. Nevertheless, the selectivity and stability of MnO_x are unsatisfied. Thus, considerable efforts have been paid to address these two issues. Commonly, the former could be improved by introducing additives like Ce or V [10,11] or changing the support [12], while for the latter, it is still unresolved despite much attempt has been made, particular for the resistance to SO_2 poisoning [13–15]. As we know, with the advance of sophisticated desulfurization technology, the content of SO_2 in most flue gas could be controlled at a rather low level ($\leq$ 50 mg/m^3). Under such circumstance, the toxic effect of SO_2 weakened tremendously. Apart from SO_2 poisoning, it is worthy to mention that great attention needs to be paid to the reaction stability in the absence of SO_2. For instance, the study from Cui *et al.* found that after 100 h of successive reaction, the NO conversion of MnO_x/TiO_2 catalyst decreased by 50 % [16]. Likewise, Zhang *et al.* reported the activity decline of Mn/CNT catalysts at 250 ℃ during the first 40 h reaction [17]. Moreover, the explicit deactivation mechanism for Mn-based catalysts under SO_2-free reaction atmosphere was ambiguous, restraining the rational development of efficient catalysts with superior

* Corresponding author at: School of Environment, Nanjing Normal University, Nanjing 210023, China.
** Corresponding author at: School of Chemistry and Chemical Engineering, Laboratory of Mesoscopic Chemistry of MOE, Nanjing University, Nanjing 210093, China.
E-mail addresses: tangcj@njnu.edu.cn (C. Tang), donglin@nju.edu.cn (L. Dong).

https://doi.org/10.1016/j.apcatb.2023.123607
Received 4 October 2023; Received in revised form 30 November 2023; Accepted 9 December 2023
Available online 18 December 2023

durability for NH_3-SCR.

Manganese oxides can present as different crystalline phases, and MnO_2, Mn_2O_3, Mn_3O_4 are typical catalysts widely explored for NH_3-SCR reaction. The activity, N_2O formation pathways and sulfur resistance of these MnO_x have been extensively investigated [18–20]. As a sharp contrast, the reaction stability of MnO_x in different phase under ideal condition has been neglected. In this study, the reaction stability of MnO_2, Mn_2O_3 and Mn_3O_4 catalysts in NH_3-SCR at the typical low temperature of 150 ℃ was examined. Results showed that despite the obtainment of better activity and selectivity for Mn_2O_3, the stability of which was inferior to MnO_2 and Mn_3O_4 in turn. Detailed physicochemical characterizations over the catalysts before and after stability test were performed to approach the reasons for deactivation. Besides, delicate experiments were designed to explore the relation between ammonium nitrates deposition and the deactivation of catalysts. With these efforts, the novel structure-activity relationship between nature of nitrates and Mn-O coordination environment was elaborated.

2. Experimental section

2.1. Catalyst preparation

MnO_2, Mn_3O_4 and Mn_2O_3 were purchased from Shanghai Aladdin and Bidepharm Biochemical Technology Co., Ltd. Ammonium nitrate (AN) was lab synthesized as a reference. The catalysts after stability test were labelled as MnO_x-R.

To ascertain the universal trend of MnO_x with crystalline structure in reaction stability, MnO_x catalysts were also prepared in laboratory and named as MnO_x-syn. MnO_2-syn catalyst was synthesized by a redox hydrothermal method [21]. A solid mixture composed of $MnSO_4{\cdot}H_2O$ (2.9140 g) and $(NH_4)_2S_2O_8$ (3.9344 g) was mixed and stirred in a Teflon lined autoclave (100 mL). The autoclave was filled with deionized water (75 mL), and then sealed and kept in an oven at 160 ℃ for 24 h and cooled to room temperature. The obtained black slurry was filtered, washed with deionized water and dried at 110 ℃ overnight. MnO_2-syn (16.9 m^2/g) was obtained by calcining the sample at 400 ℃ for 4 h. Mn_2O_3-syn (10.7 m^2/g) was obtained by directing calcining $Mn(NO_3)_2$ in air at 600 ℃ for 5 h in a tubular furnace. Mn_3O_4-syn was derived from thermal decomposition of $(CH_3COO)_2Mn{\cdot}4\,H_2O$ in a muffle furnace for a period of 24 h, maintained at a temperature of 950 ℃ [22]. Brownish black powder of Mn_3O_4 (2 m^2/g) was obtained. To exclude the effect of initial NO conversion, new Mn_2O_3 and Mn_3O_4 with excellent performance in wide work window were prepared by hydrothermal and precipitation method, respectively [21,23]. To confirm the universality of the model, α-MnO_2 was synthesized by hydrothermal method [24,25].

2.2. Activity measurement

NH_3-SCR performance and NH_3 oxidation test were measured on a fix-bed quartz reactor with internal diameter of 8 mm, and 0.1 g catalyst (40–60 mesh) was used. The simulated flue gas was composed of 500 ppm NO (when used), 500 ppm NH_3, 4 vol% O_2 and Ar as the balance gas. The total flow rate was maintained at 50 mL/min with the weight hourly space velocity (WHSV) of 30,000 $mL{\cdot}g^{-1}{\cdot}h^{-1}$. The activity test temperature was set from 60 ℃ to 240 ℃, keeping at each point for 0.5 h. The concentration of the exhaust was monitored online with a Fourier transform infrared (FTIR) spectrometer (Nicolet iS10). The lifetime test was carried out at 150 ℃ under the same condition above, but the detector was a LC-D series mass spectrometer.

The NO conversion and N_2 selectivity were calculated based on the following formulas:

$$\text{NO conversion} = 100\% \times (NO_{in} - NO_{out}) / NO_{in}$$

$$N_2\ \text{selectivity} = 100\% \times [1 - (2 \times N_2O_{out}) / (NO_{in} + NH_{3,in} - NO_{out} - NH_{3,out})]$$

2.3. Catalyst characterization

The X-ray diffraction (XRD) was utilized to identify the phase of the catalysts on a Philips X′pert Pro diffractometer with Cu Ka ($\lambda = 0.15418$ nm) radiation (2θ range:10–80°, scanning speed: 10 °/min). N_2 adsorption/desorption test was conducted on an automatic gas adsorption analyzer (Micromeritics ASAP-2020) at −196 ℃. All samples were degassed in vacuum at 150 ℃ for 4 h before test. The specific surface area was determined based on the linear portion of Brunauer-Emmett-Teller (BET) plot, while the total pore information like pore size distribution and pore volume was calculated via Barrett-Joyner Halenda (BJH) method. The X-ray photoelectron spectroscopy (XPS) measurements were carried out on PHI 5000 Versa Probe high-performance electron spectrometer with a monochromatic Al Kα as the radiation source (1486.6 eV, 15 kW). All the binding energies were calibrated using the C1s peak (BE = 284.6 eV) as standard. Transmission electron microscope (TEM) was operated on a JEM-1011 instrument operating at 200 kV.

The hydrogen temperature-programmed reduction (H_2-TPR) experiments were performed in a quartz reactor connected to a thermal conductivity detector (TCD) with H_2-Ar mixture (7 % H_2 by volume, 30 mL/min) as reducing gas. The sample (10 mg) was pretreated at 150 °C in a quartz reactor in a flow of Ar (50 mL/min) for 1 h and cooled down to the room temperature. Then reduction process was performed from room temperature to 800 °C in 7 vol% H_2/Ar gas flow of 50 mL/min at a heating rate of 10 $°C{\cdot}min^{-1}$.

NH_3-temperature programmed desorption (NH_3-TPD) measurements were carried out in the same fixed-bed quartz reactor equipped with a FTIR spectrometer to monitor outlet gas signal and the interval of spectrum collecting was set at 30 s. Prior to TPD experiments, the samples (100 mg) were pretreated at 300 °C in a flow of Ar (50 mL/min) for 0.5 h and cooled down to room temperature (30 °C). The samples were then exposed to a flow of 500 ppm NH_3/Ar (50 mL/min, Ar as the balance) at 30 °C for 1 h, followed by Ar purging for 1 h. Finally, the temperature was raised to 600 °C in Ar flow at the rate of 5 $°C{\cdot}min^{-1}$.

The content of nitrates over MnO_x as a function of reaction time was quantified by UV-Vis spectrophotometry via standard curve method. First, the MnO_x was treated with the SCR atmosphere under the same condition like stability test for 24–120 h. Second, 40 mg used catalyst was taken, and the nitrate deposited was dissolved in deionized water in a 25 mL volumetric flask. Then, the concentration of nitrates was measured by UV–vis spectrophotometer (SHIMADZU, Suzhou, China) according to 'Water quality-Determination of nitrate-nitrogen-Ultraviolet spectrophotometry' (HJ/T 346–2007). Details as follow: N in nitrates is quantitatively determined using the absorption of nitrate ions at a wavelength of 220 nm. N in dissolved organics is also absorbed at 220 nm, while nitrate ions are not absorbed at 275 nm. Therefore, another measurement was made at 275 nm to correct for the real nitrate nitrogen value.

In situ diffuse reflectance infrared Fourier transform spectroscopy (DRIFTs) was carried out on an infrared spectrometer (Nicolet-5700) equipped with an in-situ cell (HARRICK, containing KBr window) and MCT (Mercury-Cadmium-Telluride) detector cooled by liquid nitrogen. To verify the deposition was AN, the spectra of MnO_x-R and MnO_x physically mixed with 5 *wt.*% AN in N_2 at room temperature were recorded with the fresh MnO_x as a background. The formation, decomposition and reaction of AN deposition on MnO_x: each sample was pretreated at 300 °C for 0.5 h under N_2 flow, then cooled down to 150 °C to collect a background spectrum. Once the reaction gas (NO: 6000 ppm, O_2: 4 vol%, NH_3: 6000 ppm) was introduced to simulate the deposition of AN after 120 h reaction stability test, the adsorption spectra were recorded. After 1 h, the reaction gas was turned off and switched to N_2 for 30 min to examine the thermal stability for the deposition, followed by the recording of the spectrum. Then the NO (2000 ppm) was introduced again for 30 min to assess the reactivity of deposition. The

resolution was 4 cm^{-1}, and 32 scans were taken.

The AN decomposition was traced via detecting the exhaust products from heating MnO_x mixed with 5 wt% AN in Ar flow (50 mL/min) by FTIR. The samples were heated from 30 °C to 300 °C at a speed of 2 °C/min. The procedure was also conducted in the fixed-bed reactor above.

The temperature programmed surface reaction (TPSR) experiments were also performed on the same fix-bed device. 0.1 g MnO_x with 5 wt% AN was treated with the gas (500 ppm NO, balanced with Ar) from room temperature to 300 °C at a speed of 2 °C/min. Meantime, the product was detected by mass spectrometer (for N_2) and FTIR spectrometer (for NO).

3. Results and discussion

3.1. Catalytic activity and reaction stability

The result of catalytic performance as a function of reaction temperature is shown in Fig. 1a. It is obvious that the NO conversion increased with temperature until 210 ℃, and followed the order of Mn_3O_4 > Mn_2O_3 > MnO_2. When the temperature exceeded 210 ℃, decrease of NO conversion is observed, probably as a result of over oxidation of NH_3 [26]. The N_2 selectivity of three samples was exhibited in Fig. S1. It was found the best N_2 selectivity is obtained by Mn_2O_3, which is basically in agreement with reports that Mn^{3+} is conducive for N_2 formation [19,21].

To investigate the low-temperature catalytic stability of various MnO_x catalysts in NH_3-SCR, the typical temperature of 150 ℃ is chosen, and a long duration of 120 h is employed to explicitly disclose the difference in reaction stability. Besides, in view of the inherent discrepancy of these manganese oxides in NO conversion, the reaction stability was evaluated by comparing instantaneous NO conversion to initial value, and the normalized result is presented in Fig. 1b. Although no SO_2 was present in the reaction stream, deactivation still occurred. Clearly, the reaction stability manifested a close relationship with the crystalline structure of MnO_x. Mn_3O_4 displayed the best reaction stability among the three catalysts, with NO conversion efficiency changed scarcely even after successive reaction of 200 h. For the other two catalysts (MnO_2 and Mn_2O_3), certain extent of deactivation was detected, with Mn_2O_3 showed the worst reaction stability. To confirm the universality of this effect, some MnO_x catalysts from other sources were also tested and similar tendency was exhibited (Fig. S2), demonstrating the existence of phase-structure controlled reaction stability for MnO_x catalysts. Another Mn_2O_3 and Mn_3O_4 with excellent performance still were in accordance with the trend, which further excluded the effect of initial NO conversion (seen in Fig. S3).

3.2. The influence of texture property and Mn valence

To probe the reason for the different behaviors in reaction stability, XRD patterns of the catalysts before and after stability test were recorded (Fig. 2a), aiming at distinguishing any modification in crystalline phase. The catalysts could be well indexed to the crystalline structure of MnO_2 (PDF#24-0735), Mn_2O_3 (PDF#41-1442) and Mn_3O_4 (PDF#24-0734), respectively [27]. After reaction stability test, no obvious alteration of peak feature was detected, indicating well preservation of the phase structure. Besides, insignificant disturbance on the textual property of MnO_x could be confirmed from the result of N_2 physisorption (Table 1).

In addition to texture feature, the catalytic performance of MnO_x in NH_3-SCR can also be affected by its redox and chemical properties [18,21,28]. As such, H_2-TPR and XPS were conducted. All manganese oxides exhibited two H_2 consumption peaks (Fig. 2b), and the observation of greyish-green color for reduced catalysts suggested the final obtainment of Mn in MnO state [27]. For MnO_2, the low-temperature reduction at 380 ℃ could be attributed to reduction of MnO_2 to Mn_2O_3, whereas the high-temperature peak centered at 507 ℃ corresponded to the combined reduction from Mn_2O_3 to Mn_3O_4 and Mn_3O_4 to MnO [21]. For Mn_2O_3, the peaks around 453 ℃ and 581 ℃ could be ascribed to the stepwise reduction of Mn_2O_3 to Mn_3O_4 and Mn_3O_4 to MnO, respectively [21]. While for Mn_3O_4, apart from the main peak at 518 ℃ due to reduction of Mn_3O_4 to MnO, another small peak appeared at 314 ℃, which might be generated by the reduction of partial Mn^{4+} on the catalyst surface [29,30]. Notably, no distinct changes emerged for the samples before and after reaction stability test. Meanwhile, the surface average oxidation state (AOS) of Mn was estimated by the equation [31]: $AOS = 8.956–1.126\triangle E_s$, where $\triangle E_s$ represents the difference of binding energy between two Mn 3 s peaks from the XPS examination, and the results were shown in Fig. 2c and Table 1. The AOS for MnO_2, Mn_2O_3 and Mn_3O_4 was 3.9, 2.9 and 2.7, in good agreement with the anticipated value. Besides, the curves of fresh samples were in close coincidence with those of samples after reaction, indicating negligible alteration of the chemical valence of Mn. Combining the results of H_2-TPR and XPS, the effect from Mn chemical state alteration on the change of reaction stability could be ruled out.

3.3. Exploration of the deposition of ammonium nitrates

3.3.1. Qualitative and quantitative analyses of deposited ammonium nitrates on catalyst surface

As reported by Wei *et al.*, the deposition of nitrates on catalyst surface could induce blockage of active site and provoke deactivation [16]. Preliminary intuition for the deposition of ammonium nitrate during the long-term operation is evoked by the fact that some white substance was

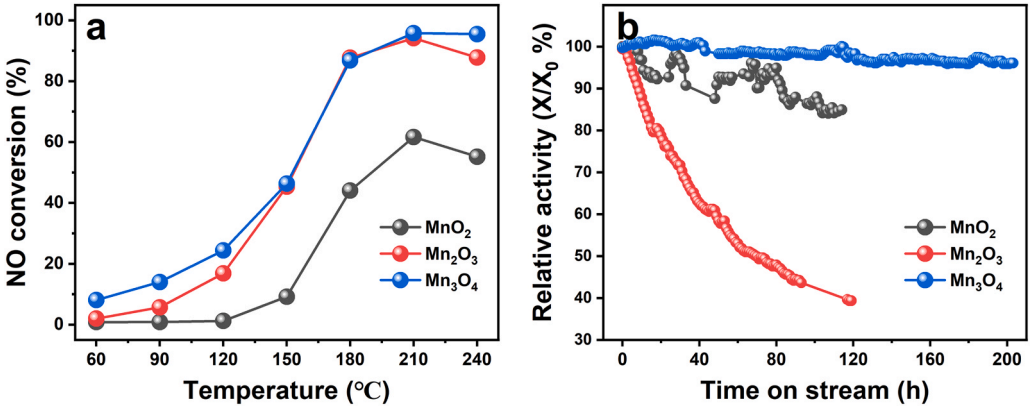

Fig. 1. The (a) catalytic activity and (b) reaction stability of MnO_2, Mn_2O_3 and Mn_3O_4 catalysts at 150 ℃. Reaction conditions: [NO] = [NH_3] = 500 ppm, [O_2] = 4 vol%, balanced with Ar, total flow rate = 50 mL·min^{-1}, WHSV = 30,000 mL·h^{-1}·g^{-1}.

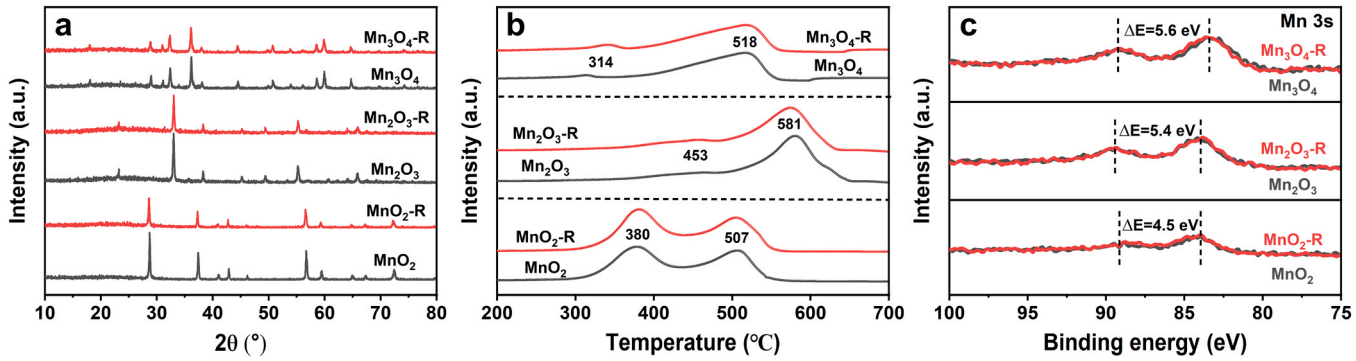

Fig. 2. The (a) XRD patterns, (b) H_2-TPR curves and (c) XPS spectra of Mn 3 s for various MnO_x catalysts before and after stability test.

Table 1
The specific surface area, pore volume and average oxidation state of Mn for samples before and after stability test.

Samples	Specific surface area (m^2/g)	Pore volume (m^3/g)	Average oxidation state of Mn
Fresh MnO_2	2.0	0.002	3.9
Spent MnO_2	1.9	0.002	3.9
Fresh Mn_2O_3	5.6	0.018	2.9
Spent Mn_2O_3	5.2	0.018	2.9
Fresh Mn_3O_4	10.1	0.065	2.7
Spent Mn_3O_4	9.3	0.064	2.7

found to coat on the wall of reactor when the catalysts were removed (seen in Fig. S4). To confirm whether the sediment was ammonium nitrate, the spent samples and those fresh MnO_x mixed with 5 wt% NH_4NO_3(AN) were characterized by in situ DRIFTS, and the result was exhibited in Fig. 3. For samples premixed with AN, two well resolved bands were observed. One band around 1380 cm^{-1} was ascribed to ion nitrates, and the other band centered between 1430–1460 cm^{-1} belonged to ammonium ions, which were typical signals of AN [32,33]. In Fig. 3a and 3c, no clear evidence for AN was shown for MnO_2-R and Mn_3O_4-R. As a distinct contrast, the bands appeared for Mn_2O_3-R in Fig. 3b, manifesting the existence of AN over the most seriously poisoned catalysts.

Our previous work reported that the nitrate species on catalyst surface could be exclusively leached into water and accurate quantification of nitrate could be fulfilled via UV-Vis spectrophotometry [34]. Here, this methodology is employed and the content of nitrates on spent MnO_x as a function of reaction time was measured. It was found from Fig. 4

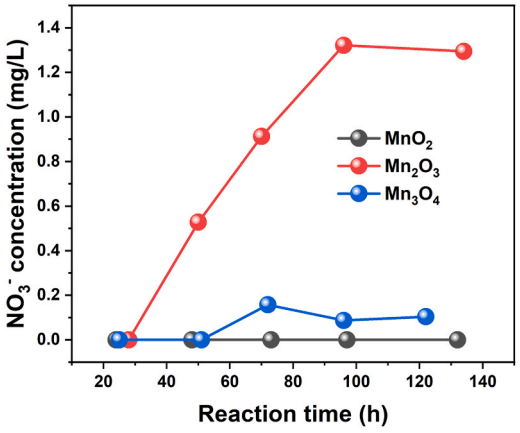

Fig. 4. The measured concentration of deposited nitrates on the three manganese oxides as a function of reaction time.

that the content of nitrates was too low to be detected over the entire test duration for MnO_2. For Mn_3O_4, the content of nitrates could not be detected until 72 h of successive reaction, and then exhibited a slightly decline tendency as the reaction time further increased. Notably, in contrast to MnO_2 and Mn_3O_4, the accumulation of nitrates on Mn_2O_3 was evident, as can be deduced from the much larger measured value from UV-Vis spectrophotometry. To further confirm the blocking effect of AN that prevented NH_3-SCR reaction on Mn sites, particularly for Mn_2O_3, the activity of the samples mixed with 5 % AN was also assessed and contrast with fresh ones at 150 ℃ (shown in Fig. S5). The NO conversion increased from 9.2 % to 17.7 % and from 46.3 % to 69.0 % for MnO_2 and Mn_3O_4 unexpectedly, while for Mn_2O_3, it decreased from 43.9 % to 11.6 %. On the basis of above results, we can propose that it is

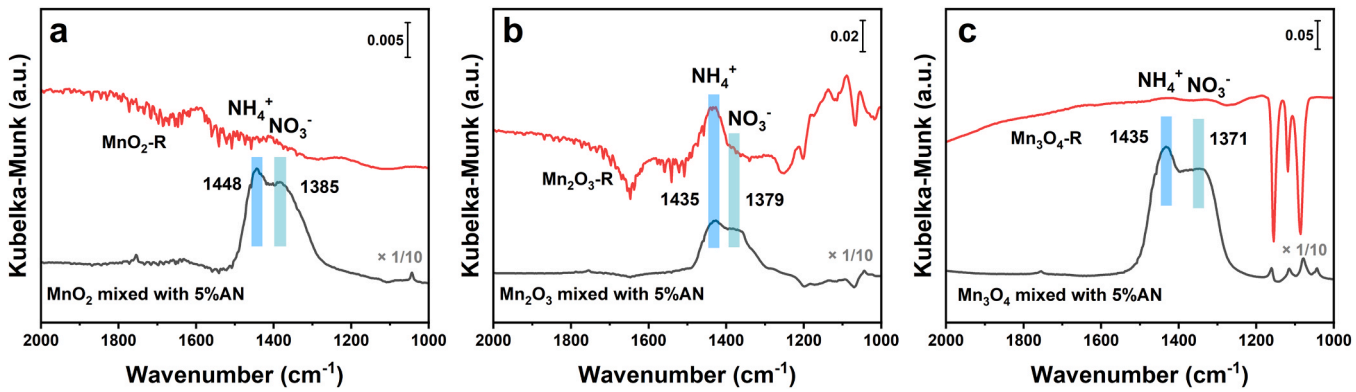

Fig. 3. In situ DRIFTS spectra of the spent samples after reaction stability test and MnO_x mixed with 5 % AN under N_2.

the formation and accumulation of ammonium nitrate species that induce the severe deactivation of Mn_2O_3.

3.3.2. The thermal stability and reactivity of ammonium nitrates

Generally, 'Fast SCR' reaction is known faster by one order of magnitude than 'Standard SCR' reaction at low temperature, which can explain the outstanding SCR performance of several metal oxides including MnO_x [35]. As an important intermediate in 'Fast-SCR', the formation of ammonium nitrate is inevitable [36]. Yet, the deposition of AN on the three manganese oxides exhibited significant variation, which led to the difference in deactivation trend. This might be relevant to the subsequent AN decomposition and reaction.

In situ DRIFTS was utilized to online record the deposition and reaction behaviors of ammonium nitrates on manganese oxide catalysts. The samples were first treated with SCR atmosphere at 150 ℃ for 60 min, then purged with N_2 for 30 min, and finally reacted with NO for 30 min. As can be seen from Fig. 5a, under SCR atmosphere, the bands around 1348 cm^{-1} and 1396 cm^{-1} could be detected for MnO_2 which were attributed to free nitrates ions (NO_3^-) and nitro-compounds coordinated via its N-atom (Mn-NO_2) [33,37]. And three inconspicuous bands at 1560 cm^{-1}, 1540 cm^{-1} and 1508 cm^{-1} were pertained to bidentate and monodentate nitrates [33,38]. Additionally, the two bands at 3150 cm^{-1} and 1432 cm^{-1} were assigned to the N-H stretching and bending vibration signal of NH_4^+ absorbed on Brønsted acid sites, respectively [39,40]. After N_2 purging, all bands attenuated and some even vanished (1560 cm^{-1}, 1540 cm^{-1} and 1508 cm^{-1}), indicating the instability of nitrates species on MnO_2. When NO was introduced, the intensity of all bands further weakened except for that of Mn-NO_2. The enhancement of nitro-compounds (Mn-NO_2, 1350 cm^{-1}) could be interpreted as reduction of nitrates with NO through the reaction [41]: Mn-NO_3^- + NO → Mn-NO_2^- + NO_2. For Mn_2O_3, the above bands also emerged in the spectra while the positions of some bands were slightly deviant (shown in Fig. 5b). After N_2 purging, the bands of monodentate and bidentate nitrates declined while the free nitrates ions signal was hardly changed, suggesting free nitrates ions were more thermally stable than nitrates coordinated to Mn sites. Unexpectedly, the nitrates absorbed on Mn_2O_3 enhanced again once exposed to NO. Besides, the characteristic bands of AN (3150 cm^{-1} and 1394 cm^{-1}) showed no obvious changes during the whole process, verifying chemical inertness of AN on Mn_2O_3 surface. As shown in Fig. 5c, the variation trend of NO_3^- and NH_4^+ over Mn_3O_4 resembled that of MnO_2. Differently, one new band at 1284 cm^{-1} related to monodentate nitrates was detected under SCR atmosphere but substantially decreased after N_2 purging and disappeared during subsequent NO treatment [33]. This suggested that the monodentate nitrates species were vivacious. Overall, the ammonium nitrate species on Mn_2O_3 were more inert than that on MnO_2 and Mn_3O_4.

The thermal stability and reactivity of ammonium nitrates on MnO_x was additionally evaluated by AN pyrolysis and NO-TPSR experiment. To track decomposition, fresh MnO_x catalysts ground with AN were heated in Ar and the evolved gases were monitored. As can be shown in Fig. 6a-c, NH_3 was first released and followed by NO_2 before 150 ℃ for MnO_2 and Mn_3O_4 samples, whilst negligible NO_2 was detected for Mn_2O_3. With temperature rising, N_2O and NO emerged as products of explosive decomposition [42]. As reported, the exothermic decomposition of pure AN took place above 200 ℃ and the explosion happened around 320 ℃ [42]. Evidently, MnO_x could catalyze the decomposition of AN like other transition metal oxides [42,43]. The evolved temperature for N_2O was thus utilized to evaluate catalytic decomposition performance of the three manganese oxides (seen in Fig. 6d). Either the onset or the peak temperature for N_2O formation followed the descending sort of Mn_3O_4 > MnO_2 > Mn_2O_3, indicating the ammonium nitrate on Mn_2O_3 was the most difficult to decompose.

The NO and N_2 signals during TPSR were collected by mass spectrometer (MS) and result was shown in Fig. 7. It could be found that the consumption of NO started before 100 ℃ accompanied with the formation of N_2. AN could react with NO via the route: NO + NH_4NO_3 → NO_2 + N_2 + $2H_2O$ [44]. Compared with that of N_2O produced in AN pyrolysis, the initial temperature for N_2 evolution was much lower, which conformed to previous studies [45,46]. Besides, the temperature for NO consumption followed the sequence: Mn_3O_4 < MnO_2 < Mn_2O_3, which was consistent with that of AN decomposition. During TPSR process, it was expected that the decomposition of AN also happened. The content of other nitrogenous compounds was documented in Fig. S6. It could be found that the existence of NO was conducive to accelerating AN decomposition and inhibiting generation of N_2O [46]. From both thermal stability and reactivity, the ammonium nitrates on Mn_2O_3 could not be eliminated and accumulate constantly, which caused the dramatic deactivation.

3.3.3. The relationship between Mn-O coordination and the feature of ammonium nitrates

From the above results, it is known that different behaviors in thermal stability and reactivity are exhibited during reaction process. To be more detailed, ammonium nitrate deposited and deactivated Mn_2O_3 severely, while it accumulated sluggishly and had limited toxic effect on MnO_2 and Mn_3O_4. Unexpectedly, acidity, which played an essential role in accelerating ammonium nitrate consumption in some literatures [45,46], had little effect herein (shown in Fig. S7). Based on the online trace of evolved gases during decomposition and reaction processes, it was confirmed that NH_4^+ in AN on Mn_2O_3 was active to be released or consumed at 150 ℃ while its counterpart-nitrates changed scarcely. Additionally, it is accepted that the breakage of N-O in nitrates was the rate determining step for both AN decomposition and reaction with NO [46,47]. In other words, the deactivation was dominated by nitrates rather than ammonium. As such, attention was paid to the factor that affect the nature of nitrates on the manganese oxides.

According to the results of in situ DRIFT, although the type of nitrates on the MnO_x catalysts was analogous, their location was not the same.

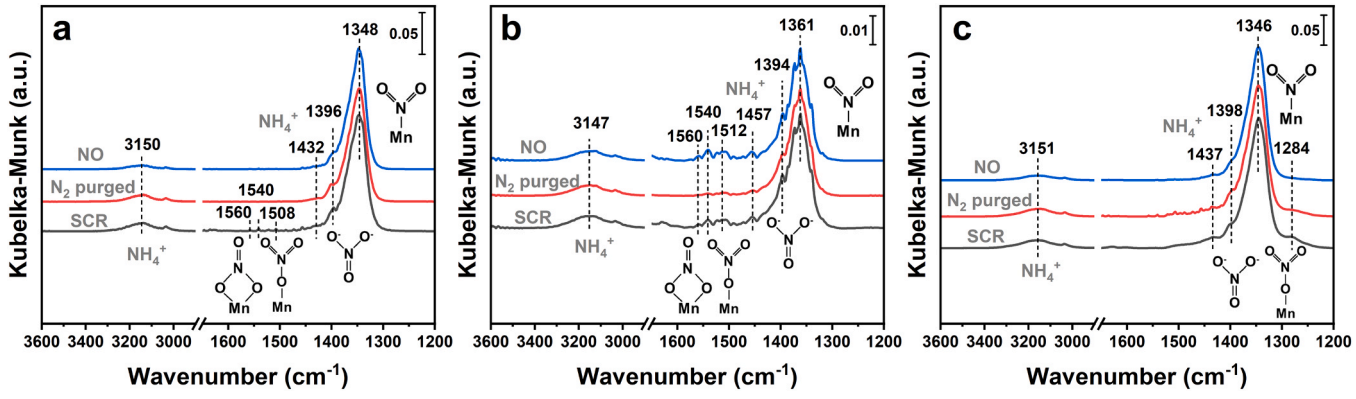

Fig. 5. In situ DRIFT spectra of ammonium nitrates formation, decomposition and reaction with NO on MnO_2 (a), Mn_2O_3 (b) and Mn_3O_4 (c) at 150 ℃.

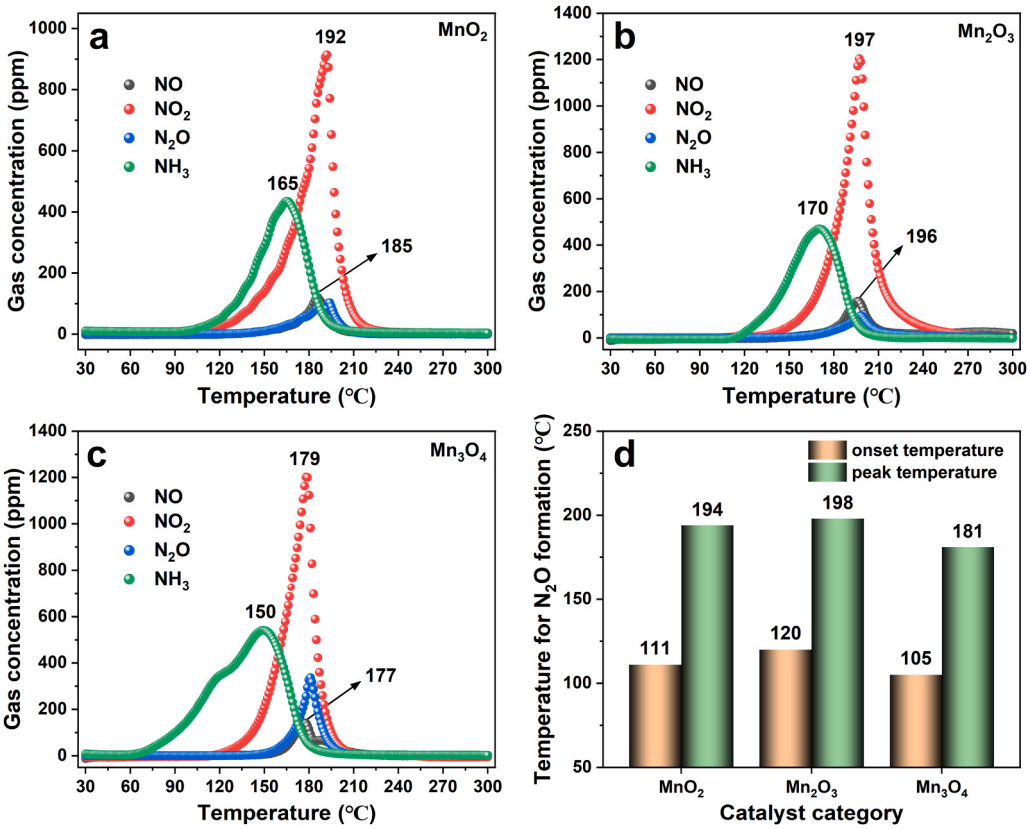

Fig. 6. Products released from AN decomposition on MnO_2 (a), Mn_2O_3 (b) and Mn_3O_4 (c) in Ar flow (40 mL/min); (d) The N_2O signal change with temperature for the three samples.

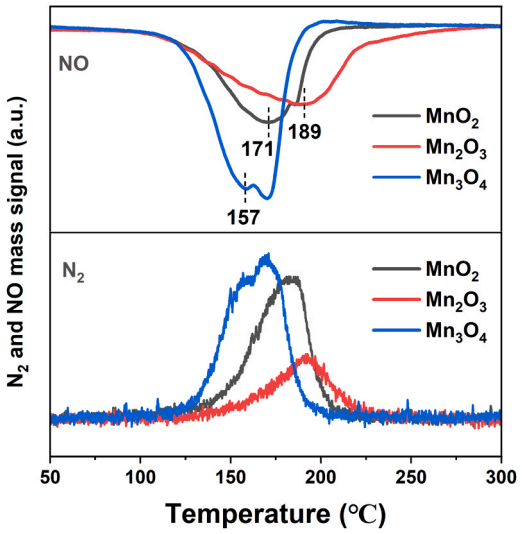

Fig. 7. The NO consumption and N_2 formation on MnO_x as function of temperature during the TPSR process.

This variance might originate from the discrepancy of manganese oxide intrinsic structure. Herein, the crystalline structures of the three manganese oxides from Inorganic Crystal Structure Database (ICSD) were adopted and filed in Fig. 8a, 8d and 8g. MnO_2 is rutile structured, in which Mn^{4+} is bonded to six equivalent O^{2-} atoms to form a mixture of edge and corner-sharing MnO_6 octahedra [48]. Mn_2O_3 is hausmannite-like structured, in which Mn^{3+} is bonded to six equivalent O^{2-} atoms to form a mixture of edge/disorder edge and corner-sharing MnO_6 octahedra [49]. For Mn_3O_4, the crystal cell belongs to spinel. In this structure, Mn^{3+} is bonded to six O^{2-} atoms to form MnO_6 octahedra, which shares corners with six equivalent MnO_4 tetrahedra and edges with six MnO_6 octahedra. Besides, Mn^{2+} is bonded to four O^{2-} atoms to form MnO_4 tetrahedra that shares corners with twelve MnO_6 octahedra [50]. The variation of Mn-O coordination environment for three manganese oxides led to the disparate nature of nitrates, which was consistent with previous reports [33,51,52].

Previously, Knözinger *et al.* and Chen's group proposed an empirical model to interpret the different OH groups on the γ-Al_2O_3, which was associated with Al-O coordination environment [53,54]. In this model, the net charge is employed as a descriptor to distinguish the acidity and alkalinity of hydroxyl. The charge value has been obtained as a sum of negative charge of the anion and all the strengths of electrostatic bonds (cation charge divided by coordination number) between the anions and adjacent cations. Like hydroxyl groups, nitrates were also bonded to metal cations sites like Mn^{n+} and tended to be ionic state in this work. Therefore, it was rational to extend this model to describe the stability of nitrates over manganese oxides. The exposed facet for these samples was measured by TEM. As shown in Fig. S8, (110), (200) and (101) facet was preferentially exposed for MnO_2, Mn_2O_3 and Mn_3O_4, respectively. The surface Mn-O configuration was obtained from the experiment and theoretical simulation [55–58]. In Fig. 8b, 8h, the coordination number of Mn^{4+} on MnO_2 (110) facet is 5, while Mn^{3+} and Mn^{2+} exposed on Mn_3O_4 (101) is coordinated by 5 and 3 oxygen atoms, respectively [55, 57]. As seen in Fig. 8e, owing to the existence of intrinsic defects and lattice distortion, the Mn^{3+} on Mn_2O_3 (200) facet was bonded to 4 oxygen atoms [56]. Based on the model, the net charge of Mn^{n+} site on MnO_2 (110), Mn_2O_3 (200) and Mn_3O_4 (101) was 2/3, 1 and 1/2, respectively. From the analyses above, free ionic nitrates were the main nitrate species. For brevity, they were chosen to explore the relationship between the nature of nitrates and the coordination configuration of MnO_x. Given that the charge of nitrate ion was −1, the net charge of

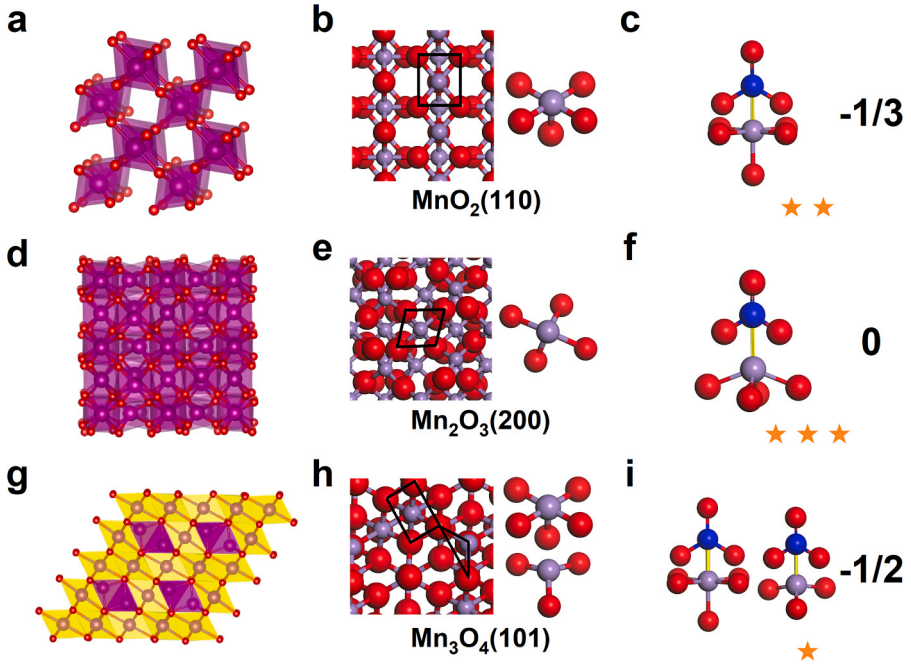

Fig. 8. The schematic diagrams of crystalline structure, preferentially exposed facet coordination configuration, constituent unit and net charge for nitrates bonded to different Mn^{n+} sites of MnO_2 (a, b, c), Mn_2O_3 (d, e, f) and Mn_3O_4 (g, h, i). The purple, red, and blue balls represent Mn, O, and N atoms, respectively. The number of pentagrams stands for stability of nitrates.

nitrates bonded at Mn^{n+} site through electrostatic force was −1/3, −1/2 and 0 (shown in Fig. 8c, 8f and 8i). According to Pauling's electrostatic valence rule, the ionic structure becomes more stable when the net charge is closer to 0 [53]. That is to say, nitrates on Mn_2O_3 were the most inert, followed by those on MnO_2 and Mn_3O_4. Consequently, AN on Mn_2O_3 could hardly decompose or be reacted off, which caused the prominent deactivation. This is in basically accordance with the experiment results. To further validate the universality of the model, α-MnO_2 was successfully synthesized and its reaction activity and stability was evaluated (shown in Fig. S9). The preferential exposed facets for α-MnO_2 was (200) and (110) [59,60]. The schematic diagrams of crystalline structure, coordination configuration in preferentially exposed facet, constituent unit and net charge for nitrates bonded to Mn^{4+} sites of α-MnO_2 are depicted in Fig. S10. It is shown that the coordination number of Mn is five for both MnO_2 (200) and MnO_2 (110), corresponding to the obtainment of net charge of −1/3 for the system. According to the proposed rule, the ammonium nitrates on catalyst surface was not stable. Therefore, its deactivation was not obvious, which agreed with the result of reaction stability test. In other words, the model proposed in this work is also suitable for α-MnO_2.

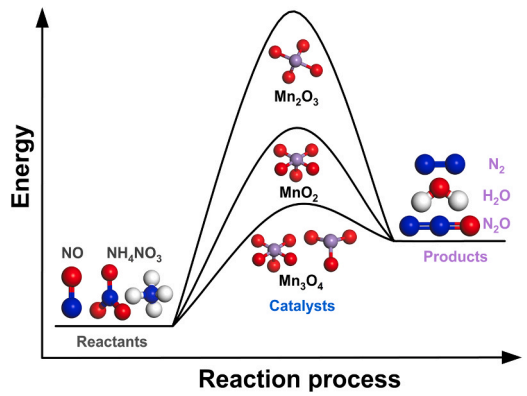

Fig. 9. The schematic diagram of the reaction process for AN on MnO_x.

To sum up, the deposition of nitrates on MnO_x was closely related to their surface coordination configuration. As shown in Fig. 9, due to its unique Mn-O coordination environment, the energy for AN decomposition or reaction on Mn_2O_3 was higher than MnO_2 and Mn_3O_4. Therefore, the ammonium nitrates accumulated and the deactivation was the most drastic among the three samples, which restricted its practical application. On the other hand, the stabilization and storage of AN can also explained why the N_2 selectivity of Mn_2O_3 was better at low temperature to a certain extent [61]. The further investigation to alleviate the deposition of nitrates was being carried out.

4. Conclusions

In this work, the relationship between reaction stability of three MnO_x catalysts (MnO_2, Mn_2O_3 and Mn_3O_4) and the Mn-O coordination was revealed for low-temperature NH_3-SCR. In the stability test, the NO conversion of Mn_2O_3 declined remarkably after 120 h reaction, followed by MnO_2, while that of Mn_3O_4 changed slightly even after 200 h reaction. The AN deposition instead of textural property and Mn valence variation was responsible for the deactivation. The category of nitrates in AN on the three manganese oxides resembled, but their performance in thermal stability and reactivity was differentiated. An empirical model to describe the stability of nitrates was proposed. According to the model, the nitrates bonded at tetra-coordinated Mn^{3+} sites on Mn_2O_3 (200) facet were stable and caused the persistent deposition of AN, which deactivated the catalysts gravely. In contrast, the penta-coordinated Mn^{4+} on MnO_2 (110) and tri-coordinated Mn^{2+} and penta-coordinated Mn^{3+} on Mn_3O_4 (101) could activate the nitrates and make it easier for AN to decompose and react with NO, thus the accumulation of AN alleviated tremendously. Besides, the continuous study to mitigate this poisonous effect was on going.

CRediT authorship contribution statement

Wang Song: Conceptualization, Data curation; Methodology, Validation, Investigation, Writing. **Qianni Cheng**: Investigation, Data curation, Revision. **Li Han**: Data curation, Revision. **Jiawei Ji**: Data

curation. **Yandi Cai**: Data curation-XPS data. **Wei Tan**: Revision, Formal analysis. **Jingfang Sun**: Investigation, Data curation, Formal analysis, Visualization. **Changjin Tang**: Conceptualization, Formal analysis, Funding acquisition, Project administration, Resources, Supervision, Writing – review & editing. **Lin Dong**: Funding acquisition, Sources, Supervision.

Declaration of Competing Interest

The authors declare that they have no known competing financial interests or personal relationships that could have appeared to influence the work reported in this paper.

Data availability

No data was used for the research described in the article.

Acknowledgement

The financial supports from the National Science Foundation of China (21976081, 21972062, 22272077, 22276097) are greatly acknowledged.

Appendix A. Supporting information

Supplementary data associated with this article can be found in the online version at doi:10.1016/j.apcatb.2023.123607.

References

[1] J.P. Chen, R.T. Yang, Role of WO_3 in mixed V_2O_5-WO_3/TiO_2 catalysts for selective catalytic reduction of nitric oxide with ammonia, Appl. Catal. A 80 (1992) 135–148, https://doi.org/10.1016/0926-860X(92)85113-P.

[2] R.T. Yang, J.P. Chen, E.S. Kikkinides, L.S. Cheng, J.E. Cichanowicz, Pillared clays as superior catalysts for selective catalytic reduction of nitric oxide with ammonia, Ind. Eng. Chem. Res. 31 (1992) 1440–1445, https://doi.org/10.1021/ie00006a003.

[3] J. Ji, N. Gao, W. Song, Y. Tang, Y. Cai, L. Han, L. Cheng, J. Sun, S. Ma, Y. Chu, C. Tang, L. Dong, Understanding the temperature-dependent H_2O promotion effect on SO_2 resistance of MnO_x-CeO_2 catalyst for SCR denitration, Appl. Catal. B Environ. 324 (2023), 122263, https://doi.org/10.1016/j.apcatb.2022.122263.

[4] D.A. Peña, B.S. Uphade, P.G. Smirniotis, TiO_2-supported metal oxide catalysts for low-temperature selective catalytic reduction of NO with NH_3: I. Evaluation and characterization of first row transition metals, J. Catal. 221 (2004) 421–431, https://doi.org/10.1016/j.jcat.2003.09.003.

[5] P.G. Smirniotis, D.A. Peña, B.S. Uphade, Low-temperature selective catalytic reduction (SCR) of NO with NH_3 by using Mn, Cr, and Cu oxides supported on hombikat TiO_2, Angew. Chem. Int. Ed. 40 (2001) 2479–2482, https://doi.org/10.1002/1521-3773(20010702)40:13<2479::AID-ANIE2479>3.0.CO;2-7.

[6] X. Li, Y. Jiang, S. Ren, Z. Chen, M. Wang, J. Li, J. Yang, H. Chen, A comparison of bifunctional MnO_x catalysts prepared via different precipitants for simultaneous removal NO and CO, Mol. Catal. 549 (2023), 113524, https://doi.org/10.1016/j.mcat.2023.113524.

[7] Z. Chen, R. Guo, S. Ren, L. Chen, X. Li, M. Wang, Comparative analysis of the dual origins of the N_2O byproduct on MnO_x, FeO_x, and $MnFeO_x$ sphere catalysts for a low-temperature SCR of NO with NH_3, J. Mater. Chem. A 10 (2022) 21474–21491, https://doi.org/10.1039/D2TA06199F.

[8] J. Liu, Y. Wei, P.-Z. Li, P. Zhang, W. Su, Y. Sun, R. Zou, Y. Zhao, Experimental and theoretical investigation of mesoporous MnO_2 nanosheets with oxygen vacancies for high-efficiency catalytic DeNO_x, ACS Catal. 8 (2018) 3865–3874, https://doi.org/10.1021/acscatal.8b00267.

[9] R. Yang, S. Peng, B. Lan, M. Sun, Z. Zhou, C. Sun, Z. Gao, G. Xing, L. Yu, Oxygen defect engineering of β-MnO_2 catalysts via phase transformation for selective catalytic reduction of NO, Small 17 (2021), 2102408, https://doi.org/10.1002/smll.202102408.

[10] S. Yang, Y. Liao, S. Xiong, F. Qi, H. Dang, X. Xiao, J. Li, N_2 selectivity of NO reduction by NH_3 over MnO_x–CeO_2: mechanism and key factors, J. Phys. Chem. C 118 (2014) 21500–21508, https://doi.org/10.1021/jp5062489.

[11] Y. Niu, T. Shang, S. Hui, X. Zhang, Y. Lei, Y. Lv, S. Wang, Synergistic removal of NO and N_2O in low-temperature SCR process with MnO_x/Ti based catalyst doped with Ce and V, Fuel 185 (2016) 316–322, https://doi.org/10.1016/j.fuel.2016.07.122.

[12] Y. Zeng, Z. Wu, L. Guo, Y. Wang, S. Zhang, Q. Zhong, Insight into the effect of carrier on N_2O formation over MnO_2/MO_x (M = Al, Si and Ti) catalysts for selective catalytic reduction (SCR) of NOx with NH_3, Mol. Catal. 488 (2020), 110916, https://doi.org/10.1016/j.mcat.2020.110916.

[13] W. Sjoerd Kijlstra, M. Biervliet, E.K. Poels, A. Bliek, Deactivation by SO_2 of MnO_x/Al_2O_3 catalysts used for the selective catalytic reduction of NO with NH_3 at low temperatures, Appl. Catal., B Environ. 16 (1998) 327–337, https://doi.org/10.1016/S0926-3373(97)00089-1.

[14] Z. Fan, J.-W. Shi, C. Niu, B. Wang, C. He, Y. Cheng, The insight into the role of Al_2O_3 in promoting the SO_2 tolerance of MnO_x for low-temperature selective catalytic reduction of NOx with NH3, Chem. Eng. J. 398 (2020), 125572, https://doi.org/10.1016/j.cej.2020.125572.

[15] K. Guo, J. Ji, W. Song, J. Sun, C. Tang, L. Dong, Conquering ammonium bisulfate poison over low-temperature NH_3-SCR catalysts: a critical review, Appl. Catal. B Environ. 297 (2021), 120388, https://doi.org/10.1016/j.apcatb.2021.120388.

[16] L. Wei, S. Cui, H. Guo, X. Ma, Y. Wan, S. Yu, The mechanism of the deactivation of MnO_x/TiO_2 catalyst for low-temperature SCR of NO, Appl. Surf. Sci. 483 (2019) 391–398, https://doi.org/10.1016/j.apsusc.2019.03.280.

[17] P. Li, T. Zhang, H. Sun, Y. Gao, Y. Zhang, Y. Liu, C. Ge, H. Chen, X. Dai, X. Zhang, Cobalt doped Fe-Mn@CNTs catalysts with highly stability for low-temperature selective catalytic reduction of NO_x, Nano Res. 15 (2022) 3001–3009, https://doi.org/10.1007/s12274-021-3932-8.

[18] F. Kapteijn, L. Singoredjo, A. Andreini, J.A. Moulijn, Activity and selectivity of pure manganese oxides in the selective catalytic reduction of nitric oxide with ammonia, Appl. Catal. B Environ. 3 (1994) 173–189, https://doi.org/10.1016/0926-3373(93)E0034-9.

[19] J. Yang, S. Ren, Y. zhou, Z. Su, L. Yao, J. Cao, L. Jiang, G. Hu, M. Kong, J. Yang, Q. Liu, In situ IR comparative study on N_2O formation pathways over different valence states manganese oxides catalysts during NH_3–SCR of NO, Chem. Eng. J. 397 (2020), 125446, https://doi.org/10.1016/j.cej.2020.125446.

[20] X. An, C. Feng, J. Liu, G. Cheng, Y. Du, Z. Fan, X. Wu, Insight into the sulfur resistance of manganese oxide for NH_3-SCR: Perspective from the valence state distributions, Appl. Surf. Sci. 592 (2022), 153223, https://doi.org/10.1016/j.apsusc.2022.153223.

[21] X. Tang, J. Li, L. Sun, J. Hao, Origination of N_2O from NO reduction by NH_3 over β-MnO_2 and α-Mn_2O_3, Appl. Catal. B Environ. 99 (2010) 156–162, https://doi.org/10.1016/j.apcatb.2010.06.012.

[22] C.S. Rani, P. Athira, N.J. John, Investigations on tri manganese tetra oxide nano particles prepared by thermal decomposition, Nanosyst.: Phys. Chem. Math. 7 (2016) 647–649, https://doi.org/10.17586/2220-8054-2016-7-4-647-649.

[23] S. Shu, J. Guo, J. Li, N. Fang, J. Li, S. Yuan, Effect of post-treatment on the selective catalytic reduction of NO with NH_3 over Mn_3O_4, Mater. Chem. Phys. 237 (2019), 121845, https://doi.org/10.1016/j.matchemphys.2019.121845.

[24] C. Wang, L. Sun, Q. Cao, B. Hu, Z. Huang, X. Tang, Surface structure sensitivity of manganese oxides for low-temperature selective catalytic reduction of NO with NH_3, Appl. Catal. B Environ. 101 (2011) 598–605, https://doi.org/10.1016/j.apcatb.2010.10.034.

[25] X. Li, S. Ren, Z. Chen, Y. Jiang, M. Wang, L. Wang, M. Liu, Unraveling the morphology and crystal plane dependence of bifunctional MnO_2 catalyst for simultaneous removal of NO and CO at low temperature, Sep. Purif. Technol. 325 (2023), 124760, https://doi.org/10.1016/j.seppur.2023.124760.

[26] H. Liu, C. You, H. Wang, Experimental and density functional theory studies on the zeolite-based Fe–Ni–W trimetallic catalyst for high-temperature NO_x selective catalytic reduction: identification of active sites suppressing ammonia over-oxidation, ACS Catal. 11 (2021) 1189–1201, https://doi.org/10.1021/acscatal.0c03949.

[27] D. Fang, J. Xie, H. Hu, H. Yang, F. He, Z. Fu, Identification of MnO_x species and Mn valence states in MnO_x/TiO_2 catalysts for low temperature SCR, Chem. Eng. J. 271 (2015) 23–30, https://doi.org/10.1016/j.cej.2015.02.072.

[28] J. Huang, H. Huang, L. Liu, H. Jiang, Revisit the effect of manganese oxidation state on activity in low-temperature NO-SCR, Mol. Catal. 446 (2018) 49–57, https://doi.org/10.1016/j.mcat.2017.12.014.

[29] F. Wang, M. Xiao, X. Ma, S. Wu, M. Ge, X. Yu, Insights into the transformations of Mn species for peroxymonosulfate activation by tuning the Mn_3O_4 shapes, Chem. Eng. J. 404 (2021), 127097, https://doi.org/10.1016/j.cej.2020.127097.

[30] F. Ji, Y. Men, J. Wang, Y. Sun, Z. Wang, B. Zhao, X. Tao, G. Xu, Promoting diesel soot combustion efficiency by tailoring the shapes and crystal facets of nanoscale Mn_3O_4, Appl. Catal. B Environ. 242 (2019) 227–237, https://doi.org/10.1016/j.apcatb.2018.09.092.

[31] M. Toupin, T. Brousse, D. Bélanger, Charge storage mechanism of MnO_2 electrode used in aqueous electrochemical capacitor, Chem. Mater. 16 (2004) 3184–3190, https://doi.org/10.1021/cm049649j.

[32] I. Nova, C. Ciardelli, E. Tronconi, D. Chatterjee, B. Bandl-Konrad, NH_3–NO/NO_2 chemistry over V-based catalysts and its role in the mechanism of the Fast SCR reaction, Catal. Today 114 (2006) 3–12, https://doi.org/10.1016/j.cattod.2006.02.012.

[33] K.I. Hadjiivanov, Identification of neutral and charged N_xO_y surface species by IR spectroscopy, Catal. Rev. 42 (2000) 71–144, https://doi.org/10.1081/CR-100100260.

[34] S. Sin, J. Ji, L. Cheng, Z. Gu, C. Tan, K. Ri, C. Tang, Quantitative discrimination of surface adsorbed NO_x species on CeO_2 via spectrophotometry for SCR denitration investigation, J. Rare Earths (2023), https://doi.org/10.1016/j.jre.2023.03.021.

[35] A. Kato, S. Matsuda, T. Kamo, F. Nakajima, H. Kuroda, T. Narita, Reaction between nitrogen oxide (NO_x) and ammonia on iron oxide-titanium oxide catalyst, J. Phys. Chem. 85 (1981) 4099–4102, https://doi.org/10.1021/j150626a029.

[36] C. Ciardelli, I. Nova, E. Tronconi, D. Chatterjee, B. Bandl-Konrad, A "Nitrate Route" for the low temperature "Fast SCR" reaction over a V_2O_5–WO_3/TiO_2 commercial catalyst, Chem. Commun. (2004) 2718–2719, https://doi.org/10.1039/B411613E.

[37] K. Hadjiivanov, H. Knözinger, Species formed after NO adsorption and NO+O_2 co-adsorption on TiO_2: an FTIR spectroscopic study, Phys. Chem. Chem. Phys. 2 (2000) 2803–2806, https://doi.org/10.1039/B002065F.

[38] W.S. Kijlstra, D.S. Brands, E.K. Poels, A. Bliek, Mechanism of the selective catalytic reduction of NO by NH_3 over MnO_x/Al_2O_3, J. Catal. 171 (1997) 208–218, https://doi.org/10.1006/jcat.1997.1788.
[39] C. Ciardelli, I. Nova, E. Tronconi, D. Chatterjee, B. Bandl-Konrad, M. Weibel, B. Krutzsch, Reactivity of NO/NO_2–NH_3 SCR system for diesel exhaust aftertreatment: Identification of the reaction network as a function of temperature and NO_2 feed content, Appl. Catal. B Environ. 70 (2007) 80–90, https://doi.org/10.1016/j.apcatb.2005.10.041.
[40] J. Li, J. Chen, R. Ke, C. Luo, J. Hao, Effects of precursors on the surface Mn species and the activities for NO reduction over MnO_x/TiO_2 catalysts, Catal. Commun. 8 (2007) 1896–1900, https://doi.org/10.1016/j.catcom.2007.03.007.
[41] L. Cao, L. Chen, X. Wu, R. Ran, T. Xu, Z. Chen, D. Weng, TRA and DRIFTS studies of the fast SCR reaction over CeO_2/TiO_2 catalyst at low temperatures, Appl. Catal. A 557 (2018) 46–54, https://doi.org/10.1016/j.apcata.2018.03.012.
[42] J.C. Oxley, J.L. Smith, E. Rogers, M. Yu, Ammonium nitrate: thermal stability and explosivity modifiers, Thermochim. Acta 384 (2002) 23–45, https://doi.org/10.1016/S0040-6031(01)00775-4.
[43] J.A. Vara, P.N. Dave, Metal oxide nanoparticles as catalyst for thermal behavior of AN based composite solid propellant, Chem. Phys. Lett. 730 (2019) 600–607, https://doi.org/10.1016/j.cplett.2019.06.048.
[44] M.P. Ruggeri, J. Luo, I. Nova, E. Tronconi, K. Kamasamudram, A. Yezerets, Novel method of ammonium nitrate quantification in SCR catalysts, Catal. Today 307 (2018) 48–54, https://doi.org/10.1016/j.cattod.2017.04.016.
[45] A. Savara, M.-J. Li, W.M.H. Sachtler, E. Weitz, Catalytic reduction of NH_4NO_3 by NO: effects of solid acids and implications for low temperature $DeNO_x$ processes, Appl. Catal. B Environ. 81 (2008) 251–257, https://doi.org/10.1016/j.apcatb.2007.12.008.
[46] H. Kubota, C. Liu, T. Toyao, Z. Maeno, M. Ogura, N. Nakazawa, S. Inagaki, Y. Kubota, K.-i Shimizu, Formation and reactions of NH_4NO_3 during transient and steady-state NH_3-SCR of NO_x over H-AFX zeolites: spectroscopic and theoretical studies, ACS Catal. 10 (2020) 2334–2344, https://doi.org/10.1021/acscatal.9b05151.
[47] C. Oommen, S.R. Jain, Ammonium nitrate: a promising rocket propellant oxidizer, J. Hazard. Mater. 67 (1999) 253–281, https://doi.org/10.1016/S0304-3894(99)00039-4.
[48] E. Hayashi, Y. Yamaguchi, K. Kamata, N. Tsunoda, Y. Kumagai, F. Oba, M. Hara, Effect of MnO_2 crystal structure on aerobic oxidation of 5-hydroxymethylfurfural to 2,5-furandicarboxylic acid, J. Am. Chem. Soc. 141 (2019) 890–900, https://doi.org/10.1021/jacs.8b09917.
[49] E. Cockayne, I. Levin, H. Wu, A. Llobet, Magnetic structure of bixbyite α-Mn_2O_3: a combined DFT+U and neutron diffraction study, Phys. Rev. B 87 (2013), 184413, https://doi.org/10.1103/PhysRevB.87.184413.
[50] P.R. Garcês Gonçalves Jr, H.A. De Abreu, H.A. Duarte, Stability, structural, and electronic properties of hausmannite (Mn_3O_4) surfaces and their interaction with water, J. Phys. Chem. C 122 (2018) 20841–20849, https://doi.org/10.1021/acs.jpcc.8b06201.
[51] K. Hadjiivanov, P. Concepción, H. Knözinger, Analysis of oxidation states of vanadium in vanadia–titania catalysts by the IR spectra of adsorbed NO, Top. Catal. 11 (2000) 123–130, https://doi.org/10.1023/A:1027269629785.
[52] M.I. Zaki, H. Kn¬ılzinger, An infrared spectroscopy study of carbon monoxide adsorption on α-chromia surfaces: probing oxidation states of coordinatively unsaturated surface cations, J. Catal. 119 (1989) 311–321, https://doi.org/10.1016/0021-9517(89)90162-0.
[53] H. Knözinger, P. Ratnasamy, Catalytic aluminas: surface models and characterization of surface sites, Catal. Rev. 17 (1978) 31–70, https://doi.org/10.1080/03602457808080878.
[54] Y. Chen, L. Zhang, Surface interaction model of γ-alumina-supported metal oxides, Catal. Lett. 12 (1992) 51–62, https://doi.org/10.1007/BF00767188.
[55] H. Yuan, N. Sun, J. Chen, J. Jin, H. Wang, P. Hu, Insight into the NH_3-assisted selective catalytic reduction of NO on β-MnO_2(110): reaction mechanism, activity descriptor, and evolution from a pristine state to a steady state, ACS Catal. 8 (2018) 9269–9279, https://doi.org/10.1021/acscatal.8b02114.
[56] Y. Xin, L. Cheng, Y. Lv, J. Jia, D. Han, N. Zhang, J. Wang, Z. Zhang, X.-M. Cao, Experimental and theoretical insight into the facet-dependent mechanisms of NO oxidation catalyzed by structurally diverse Mn_2O_3 nanocrystals, ACS Catal. 12 (2022) 397–410, https://doi.org/10.1021/acscatal.1c04357.
[57] S. Liu, L. Liu, Z. Cheng, J. Zhu, R. Yu, Surface structures of Mn_3O_4 and the partition of oxidation states of Mn, J. Phys. Chem. Lett. 12 (2021) 5675–5681, https://doi.org/10.1021/acs.jpclett.1c01422.
[58] S. Yoon, H. Seo, K. Jin, H.G. Kim, S.-Y. Lee, J. Jo, K.H. Cho, J. Ryu, A. Yoon, Y.-W. Kim, J.-M. Zuo, Y.-K. Kwon, K.T. Nam, M. Kim, Atomic reconstruction and oxygen evolution reaction of Mn_3O_4 nanoparticles, J. Phys. Chem. Lett. 13 (2022) 8336–8343, https://doi.org/10.1021/acs.jpclett.2c01638.
[59] C. He, Y. Wang, Z. Li, Y. Huang, Y. Liao, D. Xia, S. Lee, Facet engineered α-MnO_2 for efficient catalytic ozonation of odor CH_3SH: oxygen vacancy-induced active centers and catalytic mechanism, Environ. Sci. Technol. 54 (2020) 12771–12783, https://doi.org/10.1021/acs.est.0c05235.
[60] J. Luo, X. Meng, J. Crittenden, J. Qu, C. Hu, H. Liu, P. Peng, Arsenic adsorption on α-MnO_2 nanofibers and the significance of (100) facet as compared with (110), Chem. Eng. J. 331 (2018) 492–500, https://doi.org/10.1016/j.cej.2017.08.123.
[61] I. Song, H. Lee, S.W. Jeon, D.H. Kim, Controlling catalytic selectivity mediated by stabilization of reactive intermediates in small-pore environments: a study of Mn/TiO_2 in the NH_3-SCR reaction, ACS Catal. 10 (2020) 12017–12030, https://doi.org/10.1021/acscatal.0c03154.